Applied Catalysis B: Environment and Energy 347 (2024) 123784

Contents lists available at ScienceDirect

Applied Catalysis B: Environment and Energy

journal homepage: www.elsevier.com/locate/apcatb

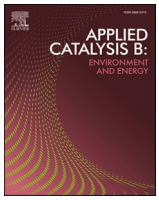

Understanding oxygen doping effects on boron nitride catalysis for efficient oxidative desulfurization of fuel oil

Peiwen Wu [a,b,*], Xin Song [a], Linjie Lu [a], Chang Deng [a], Hongying Lü [c], Linlin Chen [a,**], Haiyan Ji [d], Duanjian Tao [e], Wenshuai Zhu [a,b,*]

[a] School of Chemistry and Chemical Engineering, Jiangsu University, Zhenjiang 212013, PR China
[b] College of Chemical Engineering and Environment, State Key Laboratory of Heavy Oil Processing, China University of Petroleum-Beijing, Beijing 102249, PR China
[c] College of Chemistry and Chemical Engineering, Yantai University, Yantai 264005, PR China
[d] School of Materials Science & Engineering, Jiangsu University, Zhenjiang 212013, PR China
[e] School of Chemistry and Chemical Engineering, Jiangxi Normal University, Nanchang 330022, PR China

ARTICLE INFO

Keywords:
Oxygen-doping
Lattice oxygen
Boron nitride
Oxidative desulfurization
Fuel oil

ABSTRACT

Hexagonal boron nitride (BN) has gained increasing attention in catalysis, such as in the aerobic oxidative desulfurization (ODS) of fuel oils. Heteroatom doping has found can enhance catalytic performance, but understanding different doping modes remains a challenge for designing active catalysts. This research investigates the effect of various oxygen doping modes on the catalytic performance of BN in aerobic ODS of fuel oils. An oxygen-doped BN (BNO) is achieved through strategic modifications, and the study thoroughly examines the effects of different oxygen-doping modes. Detailed results reveal that lattice oxygen doping enhances catalytic activity, while edge hydroxylation oxygen has a negligible effect. Catalytic experiments show the superior performance of BNO, effectively removing aromatic sulfur compounds, achieving 98.4% sulfur removal, under mild conditions. This comprehensive study provides valuable insights into the effect of oxygen doping on BN catalysts and elucidates the underlying mechanisms governing their enhanced catalytic performance in ODS.

1. Introduction

As the global economy experiences rapid growth, the energy demand is escalating, accompanied by stringent criteria for energy sources [1]. Despite the emergence of numerous novel energy resources, fuel oils still serve as a primary energy source for vehicles, steamships, airplanes, and similar applications [2]. In the course of the petrochemical industry, the residual of sulfides in fuel oil products is a notable concern. Without proper treatment, these sulfides have the potential to give rise to environmental risks, including the occurrence of acidic rain, haze, and so on [3–5]. Therefore, it is crucial to proactively tackle and alleviate the potential environmental risks linked to sulfides in fuel oils by treating and eliminating them before application. Addressing these concerns, various nations and global regions have implemented stringent regulations and standards to control sulfur levels in fuel oils. In numerous countries and regions, the permissible sulfur content in fuel oils is capped at less than 10 parts per million (< 10 ppm) [6]. In this context, the desulfurization of fuel oils emerges as a pivotal undertaking. Currently, hydrodesulfurization (HDS) stands as the most commonly employed industrial process for desulfurization of fuel oils. Nonetheless, this method is limited by high energy demands and hydrogen consumption [7–9]. Furthermore, in the course of the HDS process, dibenzothiophene (DBT) and its derivatives undergo conversion into hydrogen sulfide (H_2S), a product of low economic value as well as poses the risk of environmental pollution [10,11]. Therefore, the exploration of alternative, environmentally sustainable desulfurization methods aligned with the principles of green chemistry is imperative. This approach aims to minimize environmental impact and enhance the efficient utilization of resources.

In response to the limitations of HDS, researchers have developed numerous non-HDS technologies as alternative pathways, including adsorptive desulfurization (ADS) [12,13], biodesulfurization (BDS) [14,15], extractive desulfurization (EDS) [16,17], and oxidative desulfurization (ODS) [18–24]. Within these alternative methodologies, ODS has emerged as a promising strategy due to its effectiveness in removing aromatic sulfides under mild reaction conditions [18,20]. Moreover,

* Corresponding authors at: School of Chemistry and Chemical Engineering, Jiangsu University, Zhenjiang 212013, PR China.
** Corresponding author.
E-mail addresses: wupeiwen@ujs.edu.cn (P. Wu), chenllujs@ujs.edu.cn (L. Chen), zhuws@cup.edu.cn (W. Zhu).

https://doi.org/10.1016/j.apcatb.2024.123784
Received 26 November 2023; Received in revised form 14 January 2024; Accepted 26 January 2024
Available online 29 January 2024

ODS can provide an additional advantage by converting undesirable DBT and its derivatives into valuable sulfones. Sulfones generally possess high added value and can be easily separated through a straightforward separation operation [25]. Such advantages make ODS an attractive desulfurization method for efficiently converting and removing sulfur-containing compounds from fuel oils. Especially, in ODS technologies, ODS with oxygen as the oxidizing agent has garnered considerable attention due to the abundant availability, environmentally friendly characteristics, and cost-effectiveness of oxygen. However, the challenge lies in the activation of oxygen, because of the triplet state of oxygen molecules, requiring highly active catalysts for efficient oxygen activation and the formation of reactive intermediates [26–30]. Hence, there is an imperative requirement to advance the development of a catalyst with exceptional activity to facilitate the activation of oxygen molecules for ODS of fuel oils.

Over the past a few years, hexagonal boron nitride (BN) has been found to be a promising material for its diverse and outstanding physical and chemical characteristics, including high specific surface areas, remarkable chemical stability, and exceptional thermal stability [31, 32]. These inherent properties have led to the extensive utilization of BN in diverse fields, including adsorption, biotechnology, catalysis, and related areas [33–37]. In particular, following the simultaneous groundbreaking research on employing BN as a catalyst for propane dehydrogenation by Hermans' group and for ODS by our group in 2016, there has been rapid advancement in the development of BN-based catalysts for various catalytic reactions [38,39]. Nevertheless, the inherent constraint of low catalytic activity in BN has hindered its broader applications. Under this circumstance, diverse strategies have been developed to enhance the catalytic performance of BN [40], including exfoliation for few-layered structures[41], the design of defective structures[42], hetero-atom doping[43,44], and so on. Among these strategies, heteroatom doping has garnered increasing attention as it offers the advantages of rational modification of the electronic structure of the catalyst in a controlled manner[45]. As an illustration in previous work, Wu et al. have suggested a pragmatic approach involving the incorporation of O atoms into the BN lattice, presenting a viable strategy for the modulation of its electronic structure[46]. In our prior research, we developed a polymerization strategy for synthesizing O-doped BN, to promote its adsorption capacity. The modified BN was subsequently employed in ADS processes, showcasing a notable enhancement in the efficiency of adsorbing DBT and its derivatives [47]. Inspired by these groundbreaking works, the artificial incorporation of O atoms into the BN lattice presents a promising strategy for the rational modification of electronic structures of BNs. Further investigations prove that such a modification in electronic structure can enhance the ODS efficiency of BN with O_2 as the oxidant. However, when doping O into the lattice of BN, there are two different doping modes including internal substitution or edge hydroxylation, and different doping would induce different effects on the electronic structures of BN. Distinct doping modes can either enhance or inhibit the BN catalyst, depending on the electronic structure of BN. However, deep research on the influence of various O doping modes on the catalytic ODS efficiency of BN remains a blank. Hence, it is crucial to investigate and clarify the effects of different O doping modes on the catalytic ODS performance of BN, which is indispensable for the development of highly active BN-based catalysts, especially designed for ODS applications.

In this work, an oxygen-doped boron nitride (BNO), incorporating both lattice oxygen and edge hydroxylation oxygen, was successfully synthesized via a one-pot method. The catalytic performance of the BNO in ODS with oxygen as the oxidant was systematically evaluated. Various characterizations were employed to determine the surface morphology, structure, and electronic properties of the BNO catalyst. Detailed experiments revealed that lattice oxygen plays a pivotal role in enhancing the catalytic performance of BN, while edge hydroxylation oxygen has a negligible impact on ODS performance. The introduction of oxygen atoms with higher electronegativity into the BN lattice led to a rational modification of its electronic structure. The formation of B-O bonds facilitated electron migration, resulting in the formation of electron-rich B-O active sites. The BNO catalyst exhibited exceptional ODS performance, outperforming that of unmodified BN. This study not only thoroughly discussed the relationship between the unique structure of BNO and its enhanced ODS activity, but also provides a strategy for developing highly active ODS catalysts.

2. Experimental section

2.1. Materials

All reagents employed in this study were utilized without additional purification. Boric acid (H_3BO_3) and hexamethylenetetramine (HMTA) were obtained from Sinopharm Chemical Reagent. Dibenzothiophene (DBT), 4-methyldibenzothiophene (4-MDBT), and 4,6-dimethyldibenzothiophene (4,6-DMDBT) were sourced from Sigma-Aldrich. Dodecane ($C_{12}H_{26}$) and n-Hexadecane ($C_{16}H_{34}$) were obtained from Aladdin Chemistry.

2.2. Synthesis of catalysts

2.2.1. Synthesis of BNO

The synthesis of oxygen-doped boron nitride (BNO) involved the following steps, which are modified from a previous work [48]: Initially, a solution was prepared by dissolving 0.08 mol of HMTA and 0.02 mol of H_3BO_3 in 100 mL of hot deionized water. Subsequently, the resulting mixture underwent magnetic stirring, and the solution was evaporated at 90 °C until complete evaporation of the solvent. The fully dried H_3BO_3-HMTA precursor was then transferred to a tubular furnace. The furnace was heated at a ramping rate of 10 °C/min, reaching a temperature of 1000 °C under a continuous flow of NH_3 (100 mL/min). The sample was maintained at 1000 °C for 3 h, and naturally cooled to room temperature. The obtained white powder is the BNO catalyst.

For the synthesis of BNO samples with varying oxygen concentrations, the same procedure was followed as described above, except for adjusting the molar ratio of HMTA to H_3BO_3 while keeping the amount of H_3BO_3 constant. Three different molar ratios ($n(H_3BO_3)/n$(HMTA)) were employed: 1:4, 1:8, and 1:12, resulting in the production of BNO samples designated as BNO-1, BNO-2, and BNO-3, respectively.

2.2.2. Synthesis of BNO-V

The removal of lattice oxygen from BNO to obtain BNO-V was realized by following previous procedures. The pre-synthesized BNO-2 was placed in a tubular furnace and subjected to a gradual temperature rise to 900 °C under vacuum conditions, with a heating rate of 5 °C/min. Subsequently, the furnace was maintained at 900 °C for 2 h to facilitate the calcination process, effectively removing the lattice oxygen species from BNO. The resultant sample obtained after this procedure is denoted as BNO-V [49].

2.3. Characterization

The morphological characteristics of the samples were assessed through scanning electron microscopy (SEM) and high-resolution transmission electron microscopy (HRTEM) using a JSM-7800 F electron microscope (JEOL, Japan) and JEOL-JEM-2010 (JEOL, Japan), respectively. The structural features of the BNO were determined using a D8 ADVANCE powder X-ray diffractometer (XRD) equipped with Cu Kα (k = 1.5406 Å) radiation. Fourier-transform infrared (FT-IR) spectroscopy was conducted on the Nicolet iS50 FT-IR instrument to elucidate the structural information of the sample. The specific surface area and pore diameter distribution were analyzed by nitrogen adsorption-desorption on an ASAP 2020 (Micromeritics, USA). The chemical environments of all elements in the catalysts were characterized using X-ray photoelectron spectroscopy (XPS) performed on K-Alpha at Thermo

Fisher Scientific, and the results were calibrated by C 1 s at 284.8 eV. A spin resonance (ESR) was conducted with 1,4-Benzoquinone and barbituric acid as radical traps.

2.4. Model oil desulfurization experiment

2.4.1. Preparation of model oils

The model diesel oils were prepared by dissolving different aromatic sulfides (DBT, 4-MDBT, and 4,6-DMDBT, respectively) in dodecane with concentrations of 200 ppm, respectively. Additionally, hexadecane was introduced as an internal standard at a concentration of 4000 ppm to aid in the subsequent gas chromatography (GC) analysis.

2.4.2. Oxidative desulfurization reaction process

Typically, a certain quantity of catalyst, along with 20 mL of model oil and a magnetic stir bar, are introduced into a 100 mL three-neck flask. The flask was then placed in a constant-temperature oil bath and heated to a certain temperature. A condensation reflux device is affixed to the flask. Oxygen is introduced, and continuous stirring is maintained throughout the reaction process. At regular intervals, a small sample of the upper oil phase is extracted, and 1 μL of the oil is injected into a gas chromatograph (GC) to analyze the remaining sulfur content. The desulfurization rate is computed using the following equation.

$$\text{Sulfur removal}(\%) = \frac{C_0 - C_t}{C_0} \times 100\%$$

Where C_0 represents the initial sulfur concentration and C_t represents the sulfur concentration after t time reaction.

3. Results and discussion

3.1. Characterization of BNO

In this investigation, H_3BO_3 served as the boron source, while HMTA was selected as the nitrogen source for the preparation of BNO. The presence of -OH in H_3BO_3 facilitates the reaction with protons in the amine, resulting in the formation of water and the removal of barriers for B-N bond formation, thereby lowering the energy barrier [48]. Furthermore, the establishment of B-N bonds through H_3BO_3 and amine salts requires higher energy barriers to break the B-O bonds in H_3BO_3. This process preserves a substantial quantity of B-O bonds in H_3BO_3, facilitating oxygen doping within the lattice. Conversely, oxygen atoms can also bond to the edge boron atoms of BN in the configuration of -OH, resulting in the formation of a B-OH structure.

To investigate the morphological features of BNO, a series of characterizations were carried out. Initially, SEM analysis was performed, as

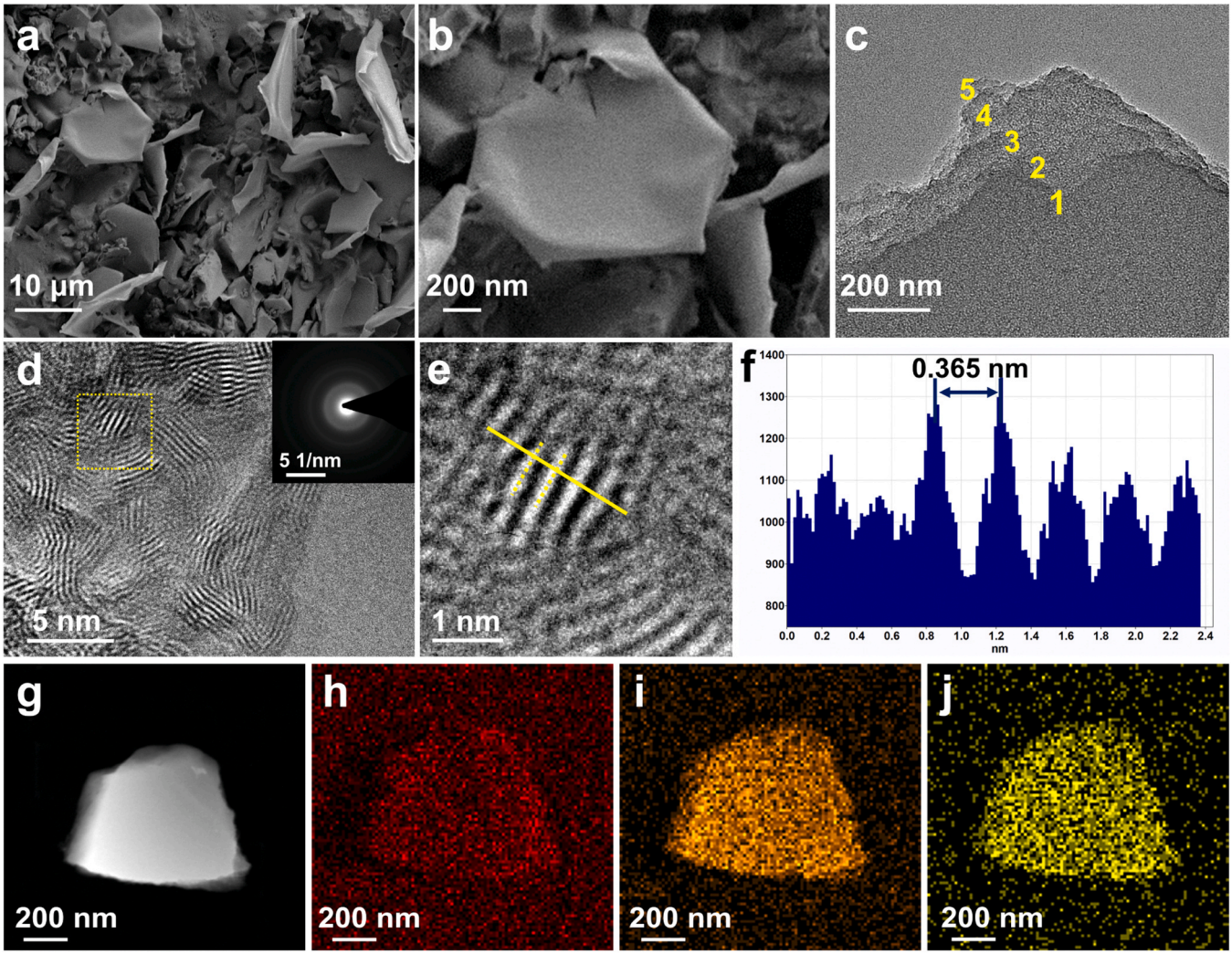

Fig. 1. Morphology characterizations and element analysis of BNO-2. a) SEM image of BNO-2; b) magnified SEM image of BNO-2; c) TEM image of BNO-2; d) HRTEM image of BNO-2; e) magnified HRTEM image of BNO-2; f) intensity profiles indicated in Fig. 1e and exemplary variations in lattice distance; g) STEM image of BNO-2 for EDS mapping; h) O element mapping of Fig. 1g; i) N element mapping of Fig. 1g; j) B element mapping of Fig. 1g.

illustrated in Fig. 1a, revealing a flake-like structure of BNO with sizes ranging from sub-micrometer to approximately 50 μm. A magnified SEM image (Fig. 1b) further demonstrated the thin-film structure of BNO, indicating its resemblance to a graphene-like structure. Subsequent TEM analysis (Fig. 1c) was conducted to observe the microstructure of BNO, confirming its similarity to pure BN with a multilayer flake structure. This affirms that the introduction of oxygen does not alter the distinctive morphology of BN. As depicted in Fig. 1c, the layers of BNO were determined to be ~5 layers, indicating a few-layered structure. The thinned layer structure of BNO enhances adsorption, thereby boosting the adsorption activity of the substrate and facilitating oxidation reactions. HRTEM analysis (Fig. 1d) was further conducted to visually observe the fine structure of BNO. The lattice fingers associated with BNO are detected in Fig. 1d, indicating a crystalline structure of the BNO. However, the lattice fingers present a short-range ordered, worm-like morphology, suggesting that the synthesized BNO is a few-layered and curly structure. Generally, BN exhibits a well-ordered two-dimensional layered structure. However, the BNO displays a two-dimensional curled structure. This is primarily due to the presence of numerous functional groups such as -OH at the edges of BNO, causing the planar curvature. Therefore, this result indicates that the synthesized BNO contains a significant amount of edge-OH groups and so on. In addition, Fig. 1d unveils that the lattice patterns on the (002) crystal plane of the prepared BNO consist of roughly 5–8 layers, aligning with the TEM characterization findings. Furthermore, selected area electron diffraction (SAED) was performed in the inset of Fig. 1d, and the results suggest that BNO-2 exhibits a polycrystalline structure, indicating a low degree of crystallinity with a disorder in long-range lattice fringe, which aligns with both XRD and HRTEM findings. Further intensity profiles indicated in Fig. 1e and exemplary variations in lattice distance, which is measured perpendicular to the (002) direction of BNO, indicate a crystal lattice spacing of ~0.365 nm of the (002) lattice plane (Fig. 1f), marginally larger than the lattice spacing of (002) lattice plane of BN (0.34 nm). Such an increase in interlayer spacing is attributed to the alteration of the lattice structure caused by the introduction of O [50, 51], proving the doping of O into the lattice. Additionally, energy-dispersive X-ray spectroscopy (EDS) analysis (Fig. 1g-i) was conducted to verify the oxygen doping in BNO. The EDS results revealed well-dispersed oxygen, nitrogen, and boron elements in the BNO samples, affirming the successful incorporation of oxygen into the BN lattice.

The FT-IR spectrum of BNO, as illustrated in Fig. 2a, offers additional structural information. The peak observed at 1385 cm^{-1} is attributed to the planar stretching vibration of the B-N bond, while the peak at 800 cm^{-1} corresponds to the bending vibration of the B-N-B bond [52]. Furthermore, the magnified FT-IR spectra in Fig. 2b reveal the emergence of a new set of infrared absorption peaks in BNO samples. Among all these newly-emerged peaks, the absorption peak at 1100 cm^{-1} corresponds to the asymmetric stretching vibration of the B-O bond in the three-coordinated BO_3, while peaks at 650 cm^{-1} and 547 cm^{-1} are indicative of the bending vibration of B-O-B [53,54]. Moreover, in the FT-IR spectra of the prepared BNO samples, peaks at ~3400 cm^{-1} and 3420 cm^{-1} are observed, attributed to -OH groups in BNO. The FT-IR characterization validates the coexistence of lattice oxygen and edge hydroxylation oxygen in BNO, aligning with the proposed formation process of BNO.

The UV-Vis spectra of BNO are displayed in Fig. S1. The spectra exhibit an absorption peak at around 240 nm for all samples, attributed to the hexagonal boron nitride phase [55]. Furthermore, two additional peaks at 320 nm and 380 nm are noted, indicative of the oxygen doping in the samples. The UV-Vis spectra further substantiate the presence of oxygen doping in BNO.

XRD analysis was performed to investigate the crystal structure of BNO with different O doping concentrations. The results, shown in Fig. 2c, reveal the presence of two distinct diffraction peaks at $2\theta = 25°$ and $2\theta = 43°$. These peaks correspond to the characteristic XRD peaks of BN, which belong to the (002) and (100) lattice planes of BN, respectively [56]. When comparing the XRD patterns of BNO catalysts with different oxygen-doping concentrations, it was observed that BNO-2 displayed the lowest intensity of the characteristic peak at $2\theta = ~24°$, indicating a higher degree of disorder or structural disruption in BNO-2.

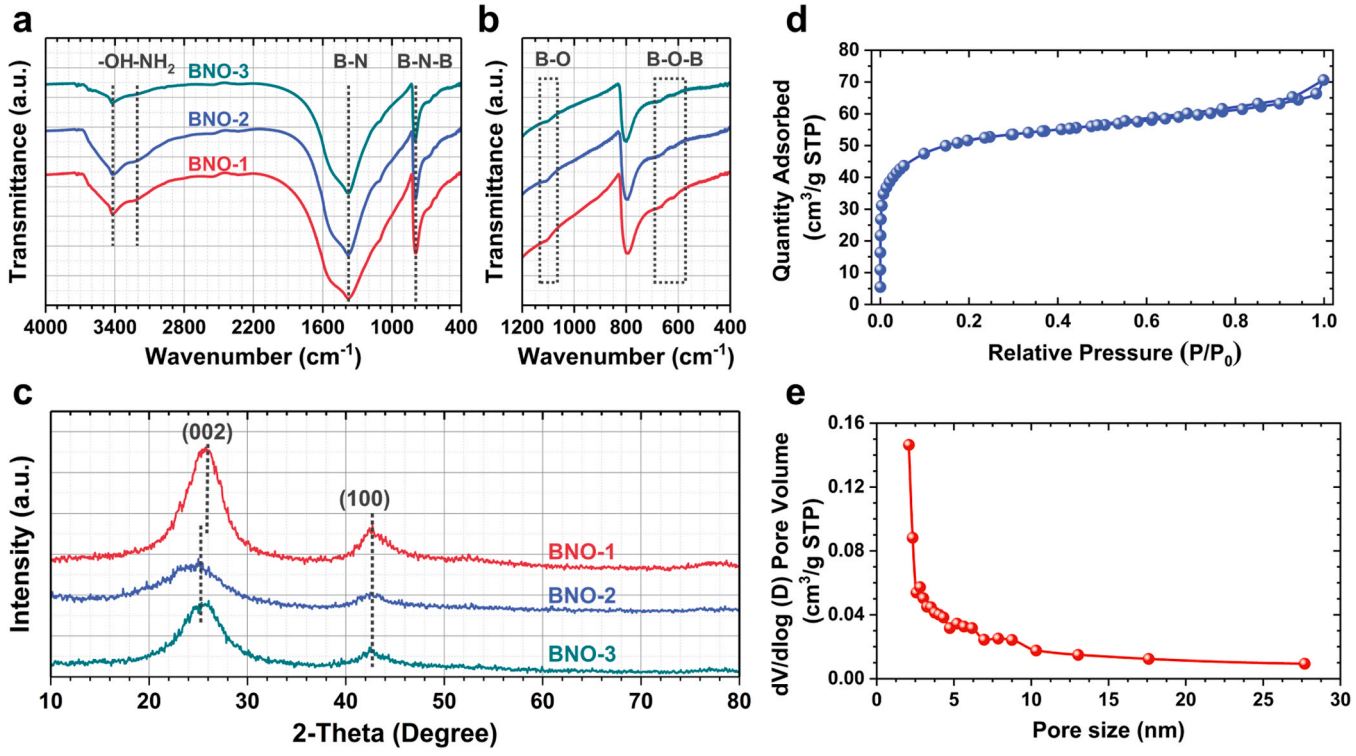

Fig. 2. Characterizations of BNO samples. a) FT-IR spectra of all BNO samples; b) magnified FT-IR spectra of all BNO samples; c) XRD patterns of all BNO samples; d) Nitrogen adsorption and desorption curve of BNO-2; and e) corresponding pore size distribution of BNO-2.

This phenomenon can be ascribed to the higher lattice oxygen concentration in BNO-2, as the introduction of oxygen atoms disrupts the order of BN atom arrangement. Additionally, the (002) lattice plane in the XRD patterns of BNO-2 and BNO-3 exhibited a noticeable downshift towards a smaller angle. According to Bragg's equation, such a downshift signifies an increase in the layer spacing of the interlayer lattice. This result is in line with the HRTEM calculations, affirming the impact of oxygen doping on the lattice and electronic structure of BN [57].

The N_2 adsorption-desorption curve and corresponding pore size distribution were performed to provide the physical structural information and pore size of BNO (Fig. 2d). The results reveal that the N_2 adsorption-desorption curve of BNO displays a typical type-I isotherm, along with a hysteresis loop within the relative pressure range of 0.65–1.0. This indicates the existence of narrow slit-shaped pores derived from the stacked nanosheets of BNO, consistent with the SEM results. The adsorption reaches saturation at relatively low pressure ($P/P_0 = 0.25$), suggesting that BNO-2 possesses a microporous and mesoporous structure. These structures contribute to the high specific surface area of BNO-2, calculated to be 180 cm^2/g. The pore size distribution analysis in Fig. 2e further affirms a centralized distribution of pore sizes around 2.5 nm. Given the small size of DBT molecules (~8 Å), such a microporous structure facilitates the construction of microchannels, enhancing the diffusion of reactants to the catalytically active sites[58].

In addition to the aforementioned characterizations, contact angle experiments were conducted by introducing oil drops onto the surface of BNO to assess its surface properties. The results, as depicted in Fig. S2, indicate that BNO possesses an excellent lipophilic nature, as evidenced by a low contact angle value. This lipophilicity suggests that BNO exhibits a high affinity for the oil phase, fostering contact between the oil phase and the catalyst surface for improved substrate mass transfer from the oil phase to the catalyst phase. The enhanced mass transfer holds significant importance in ODS, ensuring the efficient adsorption of sulfur-containing compounds onto the surface of BNO and thereby facilitating the progression of desulfurization reactions. The findings underscore that the robust lipophilicity of BNO contributes to its enhanced catalytic performance and efficiency in the ODS process [59, 60].

Generally, when oxygen atoms are doped into BN, there are two different doping modes including edge hydroxyl functional groups and lattice oxygen. Such two different doping modes induce two different chemical environments of B, including B-O-H, and B-O-B, respectively (Fig. 3a). To carefully determine the chemical composition and electronic environment of BNO catalysts, as well as differentiating the oxygen doping modes, XPS analysis of all BNO catalysts were carried out. To characterize the chemical environments of B in all BNO samples, B 1 s XPS analysis was performed in Fig. 3b-d. A thorough analysis of the B1s orbital of BNO, employing XPS peak splitting, reveals three well-defined peaks positioned at 190.0, 190.8, and 191.8 eV, corresponding to the B-N, B-O-B, and B-OH bonds in BNO, respectively [61]. The integrated analysis of XPS and FT-IR characterizations provides valuable insights into the alterations in the chemical composition and electronic environment of BNO, confirming the co-existence of distinct lattice oxygen and edge hydroxyl functional groups arising from oxygen doping. The concentrations of boron atoms in different chemical environments across all the synthesized BNO samples are compared and summarized in Figs. 3h and 3i. The findings indicate that the total quantity of boron atoms bonding with doped oxygen fluctuated with variations in the boron-nitrogen ratio, and the number of boron atoms bonding with doped oxygen increased with an increment in the HMTA content (Fig. 3h). Notably, at a boron/nitrogen ratio of 1:8 in the precursor (BNO-2), the proportion of boron atoms bonding with lattice oxygen (B-O-B) to the total boron atoms bonding with oxygen was the highest,

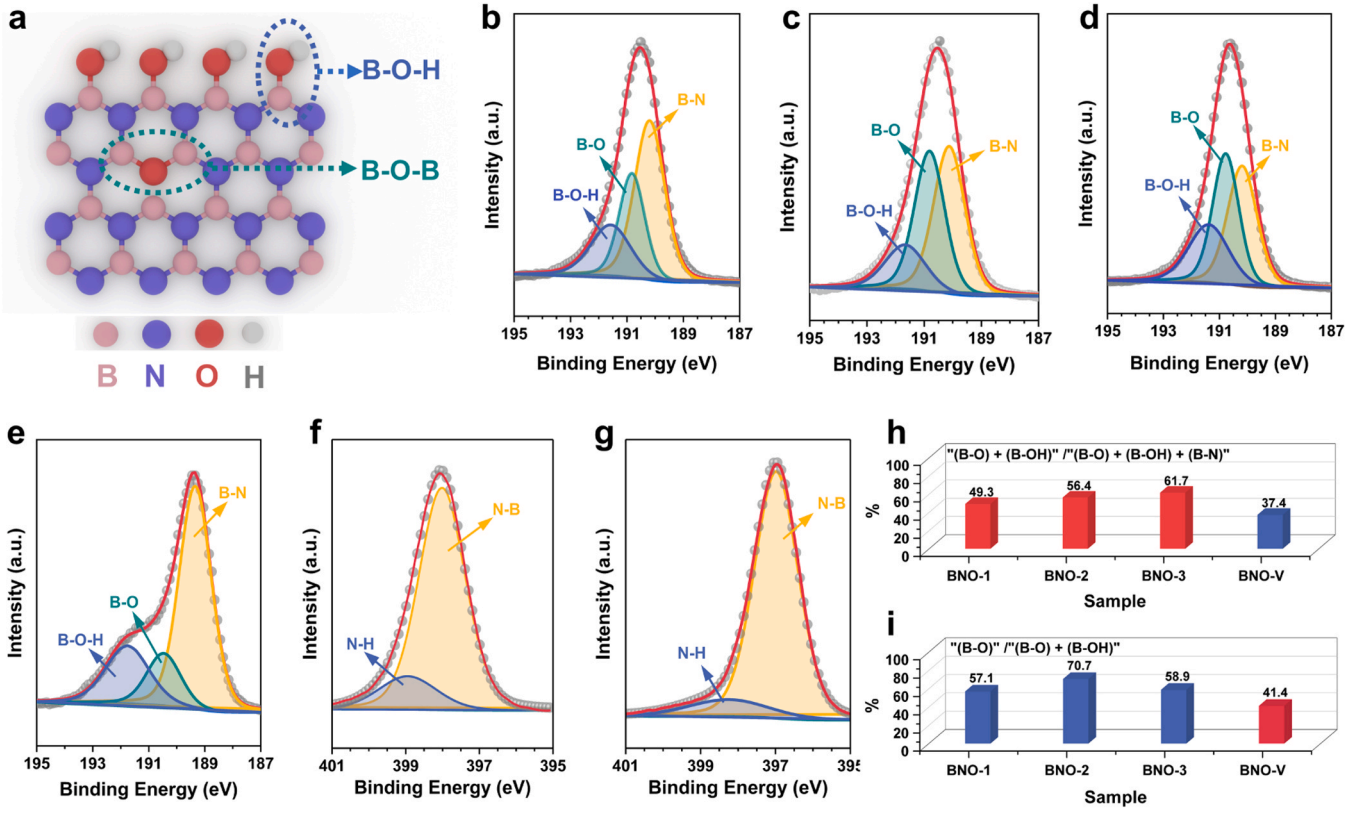

Fig. 3. XPS analysis of the prepared sample. a) schematic diagram of different oxygen doping modes in BNO; b) B1s XPS core-level spectrum of BNO-1; c) B1s XPS core-level spectrum of BNO-2; d) B1s XPS core-level spectrum of BNO-3; e) B1s XPS core-level spectrum of BNO-V; f) N1s XPS core-level spectrum of BNO-1; g) N1s XPS core-level spectrum of BNO-V; h) the ratio of boron atoms bonding with oxygen to total boron atoms; i) the ratio of boron atoms bonding with lattice to total boron atoms bonding with oxygen.

reaching 70.7% (Fig. 3i). This observation can be attributed to the random doping of oxygen atoms in the lattice. For BNO-1 and BNO-2, an increased HMTA content resulted in more B-O bonds in the plane. However, for BNO-3, the total O content increased, and the lattice oxygen reached saturation, leading to the remaining oxygen atoms forming B-OH bonds at the edges. The XPS analysis of O 1 s orbital, as shown in Figs. S3-7, also confirms such a conclusion.

Additionally, similar characterization through B 1 s XPS analysis was conducted for BNO-V, as depicted in Fig. 3e, and compared with that of BNO-2 in Figs. 3h and 3i. Under vacuum conditions, the lattice O in B-O bonds was disrupted and interacted with edge -NH_2 to produce H_2O, resulting in the removal of lattice oxygen from BNO. The results in Fig. 3e reveal that peaks for B-N, B-O-B, and B-OH, respectively, are still detectable. However, in Fig. 3h, the total concentration of boron atoms bonding with oxygen decreases, indicating the removal of oxygen atoms from BNO in BNO-V. Importantly, Fig. 3i illustrates a substantial decrease in the concentration of boron atoms bonding with lattice oxygen (B-O-B) to ~41.4%, while the content of edge hydroxylation oxygen showed no obvious decrease. confirming the removal of lattice oxygen through vacuum calcination. To substantiate the aforementioned conjecture, N 1 s XPS analysis was conducted on BNO-2 and BNO-V, as illustrated in Figs. 3f and 3g, respectively. The results indicate a decrease in the -NH_2 content after deoxygenation [49]. This further confirms the speculation that lattice oxygen reacts with edge -NH_2 groups during the removal of lattice oxygen. Furthermore, the examination of the B 1 s and N 1 s XPS spectra of BNO-V indicates a noticeable downshift towards lower binding energies, demonstrating that both boron and nitrogen atoms are positively charged in the presence of lattice oxygen. This result confirms that the introduction of oxygen modifies the electronic structure of BN, promoting enhanced electron delocalization. The increased electron delocalization facilitates electron migration, leading to the formation of active sites and ultimately

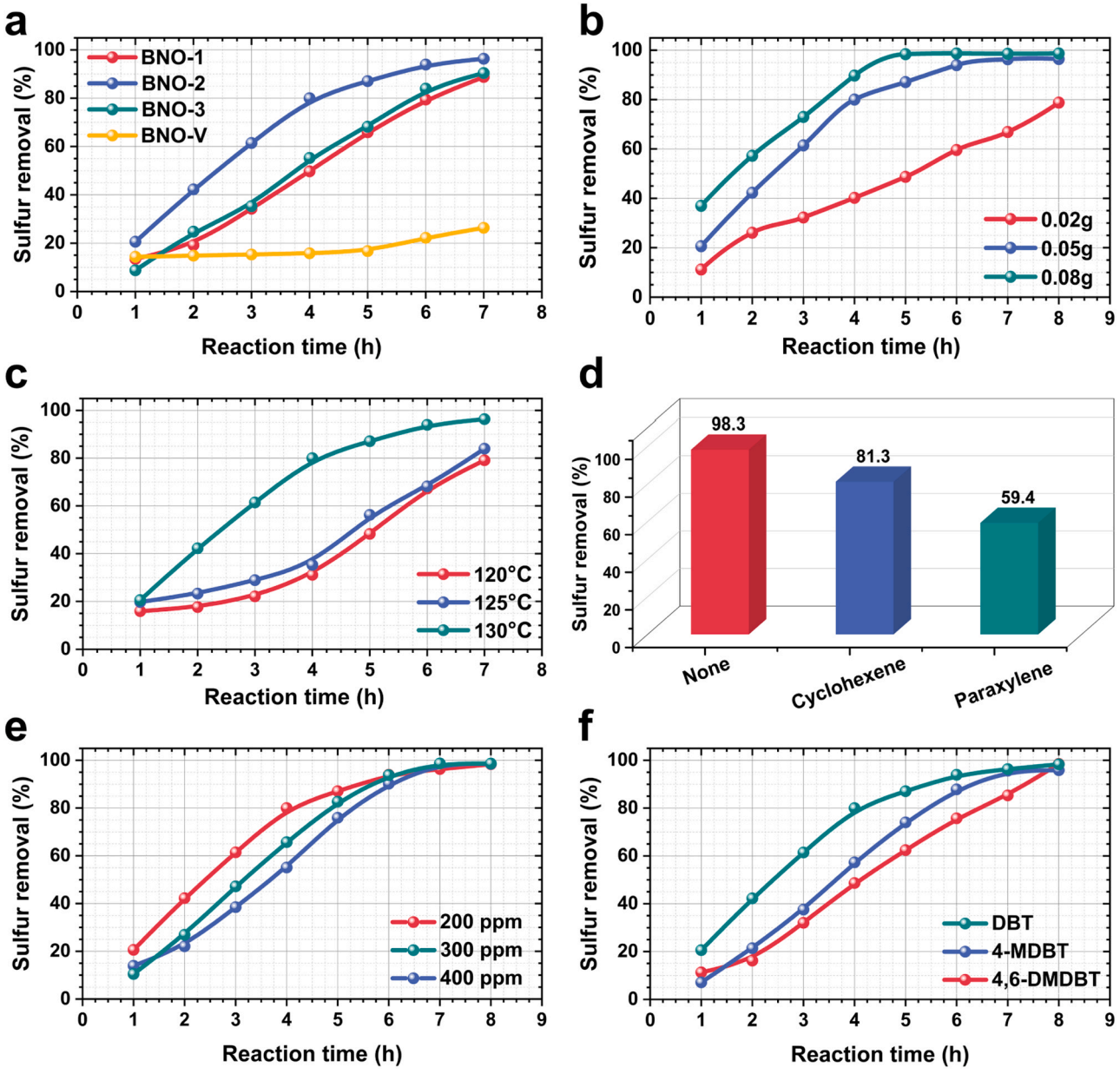

Fig. 4. Catalytic ODS performances of BNO catalysts and optimization of reaction conditions. a) Catalytic ODS performances of different BNO catalysts; b) the effect of catalyst dosage on ODS activity; c) the effect of reaction temperature on ODS activity; d) the effect of different interfering substances on ODS activity; e) the effect of initial sulfur concentration on ODS activity; f) catalytic ODS performance of BNO to different aromatic sulfides. Experimental conditions (unless otherwise specified): m(catal.) = 0.05 g, V(model oil) = 20 mL, $v(O_2)$ = 100 mL/min, T = 130 °C.

accelerating the oxidation reaction.

3.2. Catalytic performance investigation of BNO in ODS

The obtained BNO catalysts were further employed as metal-free catalysts in an ODS system using O_2 as the oxidizing agent. Initially, to emphasize the role of oxygen doping in the promotion of catalytic performances of BNOs, ODS activity experiments with O_2 as the oxidant were conducted on all BNO samples with varying oxygen concentrations (Fig. 4a). The results indicated that BNO-2 exhibited the highest catalytic activity, followed by BNO-3, while BNO-1 displayed the lowest activity. A comparative analysis reveals that the ODS activity of BNO-2 outperforms BNO-1 in terms of catalytic performance. This enhanced performance can be attributed to the higher oxygen concentration in BNO-2, effectively modulating the electronic structure of catalytically active sites and leading to improved catalytic activity. Notably, despite BNO-3 having a higher oxygen content, its catalytic activity is lower than that of BNO-2 and comparable to BNO-1. Such a result can be explained by the above XPS analysis results. The content of boron atoms bonding with lattice oxygen in BNO-3 is similar to that in BNO-2, while the content of boron atoms bonding with edge hydroxylation is in BNO-3 higher. This finding suggests that oxygen in edge hydroxylation is detrimental to catalytic activity. The XPS analysis, being combined with the ODS experiments, provides evidence that lattice oxygen is beneficial for the ODS performance of BNO, whereas edge hydroxylation oxygen hinders the catalytic activity of BNO. The BNO-2 catalyst induced 98.4% sulfur removal under optimal conditions, better than many previous works even metal-based catalysts (Table S2). To further verify the effects of different oxygen modes on the catalytic performance of BNO, BNO-2 was subjected to deoxygenation under vacuum conditions to obtain BNO-V [49], and the BNO-V was utilized as a catalyst for ODS in Fig. 4a. The results reveal that the desulfurization activity of BNO-V was only 27%, which is significantly lower than that of BNO-2. Being combined with the XPS analysis of BNO-V, which demonstrated a sharp decrease in the lattice oxygen concentration while showing no significant change in the edge hydroxylation, it further can be confirmed that it is the lattice oxygen species that significantly enhances the catalytic performance.

The optimization of reaction parameters was explored in Fig. 4b-f. Initially, the catalyst dosage was examined in Fig. 4b. The results indicate that as the BNO catalyst amount increased, the sulfur removal showed an increasing trend as well. However, the improvement in ODS catalytic activity was not substantial when the catalyst amount was increased from 0.05 g to 0.08 g. Therefore, 0.05 g was determined as the optimal catalyst dosage. Subsequently, the effect of reaction temperature was studied in Fig. 4c. The results reveal that as the reaction temperature increased, desulfurization efficiency increased as well. At the reaction temperature of 125 °C, there was only a slight enhancement in the ODS performance compared with that at 120 °C. When the temperature further increased to 130 °C, a significant improvement in the ODS performance of BNO-2 to 98.4% of sulfur removal was observed after a 7 h reaction. Therefore, 130 °C was selected as the optimized reaction temperature for the ODS system. Generally, there are some olefins and aromatics in fuel oils, which would affect the DOS performance.

To evaluate the ODS performance of BNO-2 under different environmental conditions, interference tests were conducted using common chaff interferents found in fuel oils, including p-xylene and cyclohexene. The results in Fig. 4d demonstrate that BNO-2 exhibits excellent catalytic performance even in the presence of these interfering substances, especially with the presence of p-xylene. However, with the existence of p-xylene, the ODS showed a slight decrease. Such a decrease may be assigned to competing adsorption between p-xylene and DBT.

Moreover, the effect of varying sulfur contents on catalytic ODS performance was assessed in Fig. 4e. It was noted that sulfur content has a minimal effect on the catalytic performance of the catalyst and aromatic sulfur compounds can be efficiently removed from model oils with different sulfur concentrations within 8 h. However, as the sulfur content increases, the catalytic rate decreases correspondingly. This can be attributed to the insufficient availability of catalytically active sites with an increase in sulfur content.

Furthermore, it is widely recognized that actual diesel oils not only contain DBT but also contain some other aromatic sulfur-containing compounds, such as 4-MDBT and 4,6-DMDBT. Hence, the catalytic efficiencies of BNO-2 to model oils containing diverse sulfur-containing substrates were assessed in Fig. 4f. The results, depicted in Fig. 4f, illustrate that BNO-2 demonstrates outstanding catalytic ODS performance to DBT, 4,6-DMDBT, and 4-MDBT, with the desulfurization rate following the order of DBT > 4-MDBT > 4,6-DMDBT. The difference in catalytic ODS performance to different sulfides can be attributed to the steric hindrance effect induced by the presence of methyl functional groups, influencing the catalytic activity of the BNO-2 molecules. Specifically, the steric hindrance follows the order of DBT > 4-MDBT > 4,6-DMDBT. [62]. Thus, the BNO catalyst showed the best ODS activity to DBT, and the poorest activity to 4,6-DMDBDT. In addition, to simulate the coexistence of various aromatic sulfides in real diesel oil, a model oil was prepared with a sulfide concentration of ~600 ppm by dissolving DBT, 4-MDBT, and 4,6-DMDBT in dodecane. The desulfurization efficiency of BNO-2 was further investigated, and the findings are illustrated in Fig. S7. The results reveal that after a 10 h reaction, BNO-2 achieved ~95% sulfur removal, demonstrating remarkable desulfurization performance to fuel oils containing a mixture of DBT, 4-MDBT, and 4,6-DMDBT.

3.3. Recycling performance and reaction mechanism

A recycling performance test was further conducted to assess the stability of the BNO catalyst in Fig. 5a. After each reaction cycle, the catalyst phase was separated from the upper oil phase through centrifugation at a rate of 10000 rpm. The oil phase was then removed by a tipping method, and the catalyst phase was dried in an oven at 60 °C overnight until the complete removal oil phase from the catalyst. The results in Fig. 5a indicate that BNO-2 can be recycled 4 cycles without a significant decrease in ODS performance. However, in the 4th cycle, the ODS activity of BNO decreased to ~90% of sulfur removal, displaying a declining trend in ODS performance. This decrease may be attributed to the accumulation of the ODS product, sulfone ($DBTO_2$), on the surface of BNO-2, covering the catalytically active sites. Therefore, after the 4th cycle, the BNO-2 catalyst was washed with dichloromethane to remove the adsorbed $DBTO_2$. Following the removal of $DBTO_2$, the ODS activity increased to 98.1%. This result demonstrates that the BNO-2 catalyst exhibits remarkable recycling performance in the ODS system.

Additionally, to confirm the stability of the BNO-2 catalyst during the ODS process and characterize the ODS product, FT-IR spectra of the BNO-2 catalyst before and after the ODS process were conducted in Fig. 5b. The FT-IR analysis of the reacted catalyst reveals that the characteristic structure of BNO remained unchanged after ODS. Furthermore, additional peaks observed in the FT-IR spectrum were found to correspond to the $DBTO_2$ compound. This confirms that the BNO catalyst possesses excellent stability and the ODS reaction resulted in the formation of $DBTO_2$, which has been regarded to be a high-value added product for pharmaceutical intermediates, semiconductor materials, etc. [63]. Afterward, the ODS product was carefully separated by evaporating dichloromethane to dryness during the above-mentioned recycling process, and the product was characterized by FT-IR in Fig. 5c. FT-IR analysis of the recovered sulfone indicates complete consistency with commercial-grade $DBTO_2$, confirming the simplicity and purity of the recovery process after BNO-2 converts the harmful substance DBT in fuel into the high-value-added $DBTO_2$.

To further investigate the reaction process of the catalyst, the ODS products after the ODS process were subjected to gas chromatography-mass spectrometry (GC-MS) analysis in Fig. 5d. It can be seen from the GC-MS analysis result of raw oil that a single peak at a retention time of

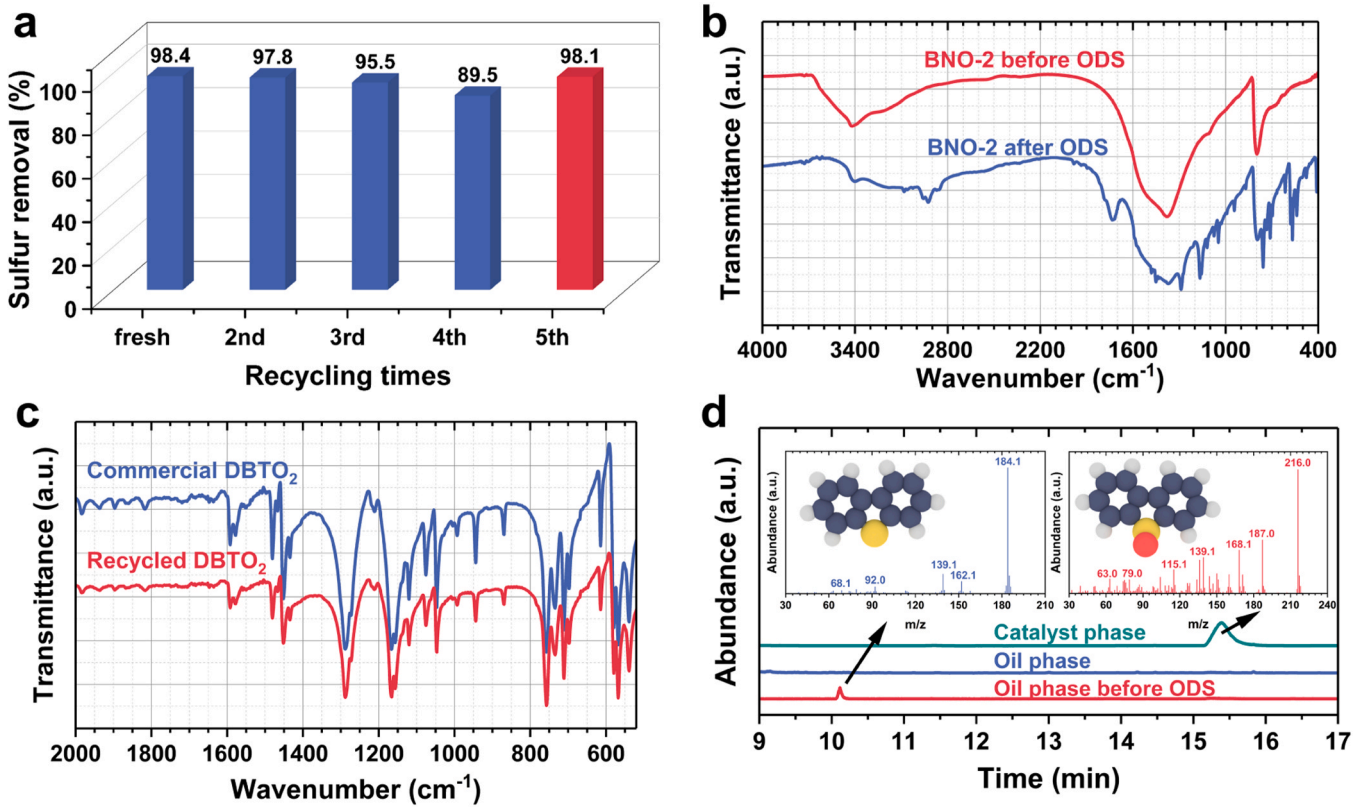

Fig. 5. Recycling performance of BNO and ODS product analysis. a) Recycling performance of the BNO catalyst; b) FT-IR spectra of BNO before and after ODS reaction; c) FT-IR spectra of recycled $DBTO_2$ and commercial $DBTO_2$; d) GC-MS analysis of oil phase before ODS, oil phase after ODS and catalyst phase after ODS. Experimental conditions of a: m(catal.) = 0.05 g, V(model oil) = 20 mL, $v(O_2)$ = 100 mL/min, T = 130 °C.

~10.2 min can be detected, which can be assigned to DBT (m/z = 180). Additionally, only $DBTO_2$ (m/z = 216.0) was observed in the catalyst phase after the ODS process. Notably, no obvious peaks for both DBT and $DBTO_2$ were observed in the oil phase after the ODS reaction, indicating the excellent oxidative desulfurization performance of BNO. These findings suggest that $DBTO_2$ is the only oxidation product of DBT and can be easily separated from the oil phase, facilitating the recovery of the sulfone product.

ESR spectroscopy was further utilized to explore the catalytically active intermediates during the ODS process using BNO-2 as the catalyst and O_2 as the oxidant. As illustrated in Fig. 6a, the separate addition of O_2 and the catalyst alone does not generate free radicals. However, when the catalyst and O_2 oxidant are introduced into the ODS system simultaneously, a distinctive signal with four peaks is detected, corresponding to the characteristic signal of superoxide free radicals ($\cdot O_2^-$). This implies that the coexistence of the catalyst and oxidant leads to the formation of $\cdot O_2^-$, which may play a crucial role in the ODS reaction [64]. Subsequently, a free radical capture experiment was conducted to further verify the formation of $\cdot O_2^-$ in the ODS process. As illustrated in Fig. 6b, p-benzoquinone (BQ) and tert-butanol (TBA) were employed as capture agents for $\cdot O_2^-$ and hydroxyl radicals (·OH), respectively. Using TBA to capture·OH left the catalytic performance of BNO unaffected. However, with the introduction of BQ to capture $\cdot O_2^-$, a significant decrease in the catalytic efficiency of the catalyst was observed. This finding suggests that the active intermediate in the aerobic catalytic ODS process is indeed $\cdot O_2^-$. Based on the above experimental findings and insights from prior literature, the introduction of lattice oxygen into BN leads to the formation of additional N-terminated edge defect sites within the boron nitride structure. These N-terminated edge defect sites serve as catalytically active centers for activating oxygen [42], significantly enhancing the catalytic ODS performance. On the other hand, the introduction of lattice oxygen induces charge redistribution within the BN surface. XPS analysis indicates a higher electron density on N atoms, making the lone pair electrons at N-terminated edge defect sites more readily transferable to the antibonding orbitals of oxygen molecules, facilitating the activation of oxygen molecules to form superoxide radicals. In summary, lattice oxygen primarily enhances the catalytic performance of BN by forming more abundant and well-regulated catalytically active site structures and modulating the charge distribution of these active sites (Fig. 6c), making the BNO more easily activate oxygen molecules to form superoxide radicals. These superoxide radicals then engage with DBT to produce $DBTO_2$, ultimately driving the desulfurization process.

4. Conclusion

In summary, an oxygen-doped boron nitride (BNO) catalyst was engineered and the characterization of BNO demonstrates that BNO possesses a few-layered structure with a remarkable specific surface area, enhancing substrate adsorption. Crucially, lattice oxygen doping has been identified as conducive to catalytic oxidative desulfurization (ODS) performance, while edge hydroxylation oxygen has a deactivating effect. Detailed experiments have elucidated that lattice oxygen doping induces B-O-B bonds in the lattice, facilitating electron migration and enhancing desulfurization efficiency, achieving a remarkable sulfur removal of up to 98.4% within 7 h. The BNO catalyst showed excellent ODS activities in oils containing different aromatic sulfides or containing aromatic sulfides with different concentrations. Furthermore, the conversion of DBT to $DBTO_2$, a valuable product, highlights the potential for high-value transformations. The catalyst also demonstrates commendable cyclic performance and stability. This study introduces an innovative approach to the rational design of boron nitride catalysts, paving the way for metal-free modifications of boron nitride.

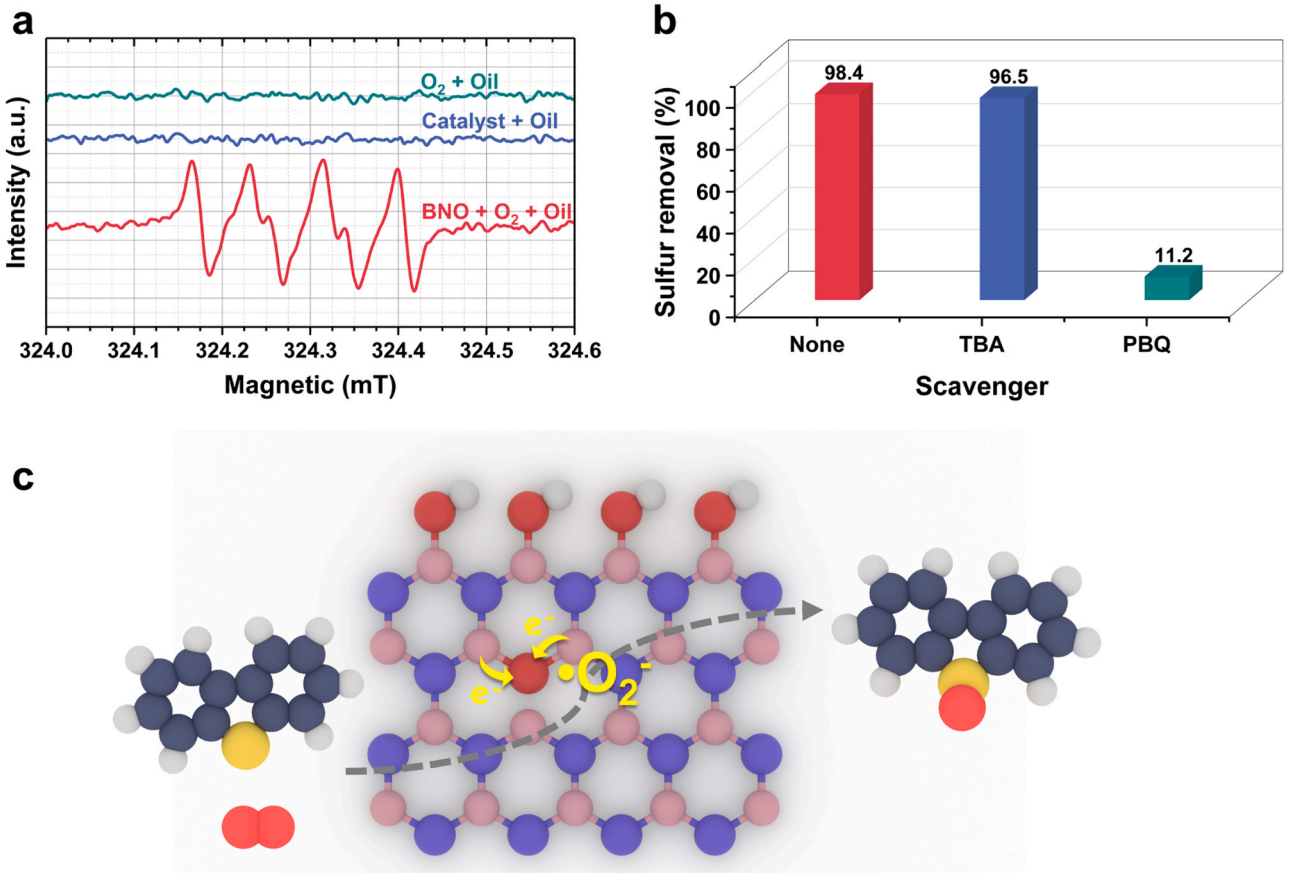

Fig. 6. Investigation of ODS reaction mechanism over BNO. a) ESR analysis of different ODS systems; b) Free radical trapping experiments using different radical scavengers; c) proposed reaction mechanism. Experimental conditions of b: m(catal.) = 0.05 g, V(model oil) = 20 mL, $v(O_2)$ = 100 mL/min, T = 130 °C.

CRediT authorship contribution statement

Peiwen Wu: Writing – review & editing, Writing – original draft, Visualization, Methodology, Investigation, Funding acquisition, Data curation, Conceptualization. **Xin Song:** Writing – original draft, Visualization, Methodology, Investigation, Data curation. **Linjie Lu:** Writing – review & editing, Validation, Investigation, Data curation. **Chang Deng:** Writing – review & editing, Validation, Methodology, Formal analysis. **Hongying Lü:** Writing – review & editing, Visualization. **Linlin Chen:** Writing – review & editing, Writing – original draft, Supervision, Conceptualization. **Haiyan Ji:** Writing – review & editing, Visualization, Funding acquisition. **Duanjian Tao:** Writing – review & editing, Visualization. **Wenshuai Zhu:** Writing – review & editing, Supervision, Funding acquisition, Conceptualization.

Declaration of Competing Interest

The authors declare that they have no known competing financial interests or personal relationships that could have appeared to influence the work reported in this paper.

Data availability

Data will be made available on request.

Acknowledgements

All authors appreciate the financial support from the National Key R&D Program of China (No. 2022YFA1504404, 2022YFA1504403), the National Natural Science Foundation of China (No. 22178154, 22008094), Natural Science Foundation of Jiangsu Province (No. BK20230068, BK20221367).

Appendix A. Supporting information

Supplementary data associated with this article can be found in the online version at doi:10.1016/j.apcatb.2024.123784.

References

[1] X. Zhou, T. Wang, H. Liu, X. Gao, C. Wang, G. Wang, Desulfurization through photocatalytic oxidation: a critical review, ChemSusChem 14 (2021) 492–511, https://doi.org/10.1002/cssc.202002144.
[2] R.A. Omar, N. Verma, Review of adsorptive desulfurization of liquid fuels and regeneration attempts, Ind. Eng. Chem. Res. 61 (2022) 8595–8606, https://doi.org/10.1021/acs.iecr.2c01426.
[3] K. Yu, W. Kong, Z. Zhao, A. Duan, L. Kong, X. Wang, Hydrodesulfurization of dibenzothiophene and 4,6-dimethyldibenzothiophene over NiMo supported on yolk-shell silica catalysts with adjustable shell thickness and yolk size, J. Catal. 410 (2022) 128–143, https://doi.org/10.1016/j.jcat.2022.04.012.
[4] Z. Safaei Mahmoudabadi, A. Rashidi, M. Panahi, New approach to unsupported ReS_2 nanorod catalyst for upgrading of heavy crude oil using methane as hydrogen source, Int. J. Hydrog. Energy 46 (2021) 5270–5285, https://doi.org/10.1016/j.ijhydene.2020.11.077.
[5] J. He, P. Wu, L. Chen, H. Li, M. Hua, L. Lu, Y. Wei, Y. Chao, S. Zhou, W. Zhu, H. Li, Dynamically-generated TiO_2 active site on MXene Ti_3C_2: boosting reactive desulfurization, Chem. Eng. J. 416 (2021) 129022, https://doi.org/10.1016/j.cej.2021.129022.
[6] Y. Wei, P. Wu, J. Luo, D. Tao, C. Peng, L. Dai, L. Wang, H. Li, W. Zhu, Binary molten salts mediated defect engineering on hexagonal boron nitride catalyst with long-term stability for aerobic oxidative desulfurization, Appl. Surf. Sci. 529 (2020) 149724, https://doi.org/10.1016/j.apsusc.2021.149724.
[7] L. Lu, J. He, P. Wu, Y. Sun, M. Hua, P. Cui, W. Zhu, H. Li, Z. Liu, C. Xu, Stable Au nanoparticles confined in boron nitride shells for optimizing oxidative desulfurization, Nano Res. 16 (2022) 12076–12083, https://doi.org/10. 1007/s12274-022-5113-9.

[8] W. Zhou, L. Yang, L. Liu, Z. Chen, A. Zhou, Y. Zhang, X. He, F. Shi, Z. Zhao, Synthesis of novel NiMo catalysts supported on highly ordered TiO_2-Al_2O_3 composites and their superior catalytic performance for 4,6-dimethyldibenzothiophene hydrodesulfurization, Appl. Catal. B Environ. 268 (2020) 118428, https://doi.org/10.1016/j.apcatb.2019.118428.

[9] D. Ryaboshapka, L. Piccolo, M. Aouine, P. Bargiela, V. Briois, P. Afanasiev, Ultradispersed (Co)Mo catalysts with high hydrodesulfurization activity, Appl. Catal. B Environ. 302 (2022) 120831, https://doi.org/10.1016/j.apcatb.2021.120831.

[10] S.S. Bello, C. Wang, M. Zhang, H. Gao, Z. Han, L. Shi, F. Su, G. Xu, A review on the reaction mechanism of hydrodesulfurization and hydrodenitrogenation in heavy oil upgrading, Energy Fuel 35 (2021) 10998–11016, https://doi.org/10.1021/acs.energyfuels.1c01015.

[11] Z. Liu, W. Han, D. Hu, S. Sun, A. Hu, Z. Wang, Y. Jia, X. Zhao, Q. Yang, Effects of Ni–Al_2O_3 interaction on NiMo/Al_2O_3 hydrodesulfurization catalysts, J. Catal. 387 (2020) 62–72, https://doi.org/10.1016/j.jcat.2020.04.008.

[12] S. Gooneh-Farahani, M. Anbia, A review of advanced methods for ultra-deep desulfurization under mild conditions and the absence of hydrogen, J. Environ. Chem. Eng. 11 (2023) 108997, https://doi.org/10.1016/j.jece.2022.108997.

[13] T. Zhou, S. Wang, C. Zhang, Y. Yao, Y. Chen, S. Lu, X. Liao, Preparation of Ti-MOFs for efficient adsorptive desulfurization: synthesis, characterization, and adsorption mechanisms, Fuel 339 (2023) 127396, https://doi.org/10.1016/j.fuel.2023.127396.

[14] A. Dejaloud, A. Habibi, F. Vahabzadeh, DBT desulfurization by Rhodococcus erythropolis PTCC 1767 in aqueous and biphasic systems, Chem. Pap. 74 (2020) 3605–3615, https://doi.org/10.1007/s11696-020-01191-5.

[15] H.N. Nassar, S.S. Abu Amr, N.S. El-Gendy, Biodesulfurization of refractory sulfur compounds in petro-diesel by a novel hydrocarbon tolerable strain Paenibacillus glucanolyticus HN4, Environ. Sci. Pollut. Res. Int. 28 (2021) 8102–8116, https://doi.org/10.1007/s11356-020-11090-7.

[16] N. Khan, V.C. Srivastava, Quaternary ammonium salts-based deep eutectic solvents: utilization in extractive desulfurization, Energy Fuel 35 (2021) 12734–12745, https://doi.org/10.1021/acs.energyfuels.1c01220.

[17] M. Dana, S. Shahhosseini, M.A. Sobati, A.R. Ansari, M. Asadollahzadeh, Optimization of extractive desulfurization of diesel oil in a continuous Oldshue–Rushton column pilot plant, Energy Fuel 34 (2019) 1041–1052, https://doi.org/10.1021/acs.energyfuels.9b02793.

[18] P. Wu, Y. Sun, L. Chen, Q. Jia, J. He, W. Ma, L. Lu, Y. Chao, L. Fan, W. Zhu, Heteroatom bridging strategy in carbon-based catalysts for enhanced oxidative desulfurization performance, Inorg. Chem. 61 (2022) 633–642, https://doi.org/10.1021/acs.inorgchem.1c03356.

[19] M.Y. Yu, J. Yang, T.T. Guo, J.F. Ma, Efficient catalytic oxidative desulfurization toward thioether and sulfur mustard stimulant by polyoxomolybdate-Resorcin[4]arene-based metal-organic materials, Inorg. Chem. 59 (2020) 4985–4994, https://doi.org/10.1021/acs.inorgchem.0c00225.

[20] P. Wu, L. Lu, J. He, L. Chen, Y. Chao, M. He, F. Zhu, X. Chu, H. Li, W. Zhu, Hexagonal boron nitride: a metal-free catalyst for deep oxidative desulfurization of fuel oils, Green Energy Environ. 5 (2020) 166–172, https://doi.org/10.1016/j.gee.2020.03.004.

[21] P. Wu, X. Song, L. Chen, L. He, Y. Wu, D. Tao, J. He, C. Deng, L. Lu, Y. Chao, M. Hua, W. Zhu, Few-layered hexagonal boron nitride nanosheets stabilized Pt NPs for oxidation promoted adsorptive desulfurization of fuel oil, Green Energy Environ. (2022), https://doi.org/10.1016/j.gee.2022.08.003.

[22] A. Rajendran, H.-X. Fan, T.-Y. Cui, J. Feng, W.-Y. Li, Octamolybdates containing MoV and MoVI sites supported on mesoporous tin oxide for oxidative desulfurization of liquid fuels, J. Clean. Prod. 334 (2022) 130199, https://doi.org/10.1016/j.jclepro.2021.130199.

[23] I. Shafiq, S. Shafique, P. Akhter, G. Abbas, A. Qurashi, M. Hussain, Efficient catalyst development for deep aerobic photocatalytic oxidative desulfurization: recent advances, confines, and outlooks, Catal. Rev. 64 (2021) 789–834, https://doi.org/10.1080/01614940.2020.1864859.

[24] P. Wang, L. Jiang, X. Zou, H. Tan, P. Zhang, J. Li, B. Liu, G. Zhu, Confining polyoxometalate clusters into porous aromatic framework materials for catalytic desulfurization of dibenzothiophene, ACS Appl. Mater. Interfaces 12 (2020) 25910–25919, https://doi.org/10.1021/acsami.0c05392.

[25] P. Wu, C. Deng, P. Liu, F. Liu, L. Chen, B. Wang, W. Zhu, C. Xu, An ultra-stable high entropy metal nitride for aerobic oxidative desulfurization and source recovery of aromatic sulfides from fuel oils, Chem. Eng. J. 474 (2023) 145850, https://doi.org/10.1016/j.cej.2023.145850.

[26] I. Mahboob, I. Shafiq, S. Shafique, P. Akhter, U.-e-S. Amjad, M. Hussain, Y.-K. Park, Effect of active species scavengers in photocatalytic desulfurization of hydrocracker diesel using mesoporous Ag_3VO_4, Chem. Eng. J. 441 (2022) 136063, https://doi.org/10.1016/j.cej.2022.136063.

[27] M. Chi, T. Su, L. Sun, Z. Zhu, W. Liao, W. Ren, Y. Zhao, H. Lü, Biomimetic oxygen activation and electron transfer mechanism for oxidative desulfurization, Appl. Catal. B Environ. 275 (2020) 119134, https://doi.org/10.1016/j.apcatb.2020.119134.

[28] L. Sun, T. Su, P. Li, J. Xu, N. Chen, W. Liao, C. Deng, W. Ren, H. Lü, Extraction coupled with aerobic oxidative desulfurization of model diesel using a B-type Anderson polyoxometalate catalyst in ionic liquids, Catal. Lett. 149 (2019) 1888–1893, https://doi.org/10.1007/s10562-019-02791-x.

[29] B. Yuan, X. Li, Y. Sun, A short review of aerobic oxidative desulfurization of liquid fuels over porous materials, Catalysts 12 (2022) 129, https://doi.org/10.3390/catal12020129.

[30] Y. Zou, C. Wang, H. Chen, H. Ji, Q. Zhu, W. Yang, L. Chen, Z. Chen, W. Zhu, Scalable and facile synthesis of V_2O_5 nanoparticles via ball milling for improved aerobic oxidative desulfurization, Green Energy Environ. 6 (2021) 169–175, https://doi.org/10.1016/j.gee.2020.10.005.

[31] J. Tian, J. Tan, M. Xu, Z. Zhang, S. Wan, S. Wang, J. Lin, Y. Wang, Propane oxidative dehydrogenation over highly selective hexagonal boron nitride catalysts: the role of oxidative coupling of methyl, Sci. Adv. 5 (2019) eaav8063, https://doi.org/10.1126/sciadv.aav8063.

[32] Z. Zhang, J. Tian, X. Wu, I. Surin, J. Perez-Ramirez, P. Hemberger, A. Bodi, Unraveling radical and oxygenate routes in the oxidative dehydrogenation of propane over boron nitride, J. Am. Chem. Soc. 145 (2023) 7910–7917, https://doi.org/10.1021/jacs.2c12970.

[33] M. Kim, S.W. Moon, G. Kim, S.I. Yoon, K. Kim, S.K. Min, H.S. Shin, Effect of Pt crystal surface on hydrogenation of monolayer h-BN and its conversion to graphene, Chem. Mater. 32 (2020) 4584–4590, https://doi.org/10.1021/acs.chemmater.0c00736.

[34] L. He, J. Zeng, Y. Huang, X. Yang, D. Li, Y. Chen, X. Yang, D. Wang, Y. Zhang, Z. Fu, Enhanced thermal conductivity and dielectric properties of h-BN/LDPE composites, Materials 13 (2020) 4738, https://doi.org/10.3390/ma13214738.

[35] Y. Hu, Y. Yin, G. Ding, J. Liu, H. Zhou, W. Feng, G. Zhang, D. Li, High thermal conductivity in covalently bonded bi-layer honeycomb boron arsenide, Mater. Today Phys. 17 (2021) 100346, https://doi.org/10.1016/j.mtphys.2021.100346.

[36] H. Chen, D.E. Jiang, Z. Yang, S. Dai, Engineering nanostructured interfaces of hexagonal boron nitride-based materials for enhanced catalysis, Acc. Chem. Res. 56 (2023) 52–65, https://doi.org/10.1021/acs.accounts.2c00564.

[37] M. Qu, G. Qin, J. Fan, A. Du, Q. Sun, Boron-rich boron nitride nanomaterials as efficient metal-free catalysts for converting CO_2 into valuable fuel, Appl. Surf. Sci. 555 (2021) 149652, https://doi.org/10.1016/j.apsusc.2021.149652.

[38] J.T. Grant, C.A. Carrero, F. Goeltl, J. Venegas, P. Mueller, S.P. Burt, S.E. Specht, W. P. McDermott, A. Chieregato, I. Hermans, Selective oxidative dehydrogenation of propane to propene using boron nitride catalysts, Science 354 (2016) 1570–1573, https://doi.org/10.1126/science.aaf7885.

[39] P. Wu, W. Zhu, Y. Chao, J. Zhang, P. Zhang, H. Zhu, C. Li, Z. Chen, H. Li, S. Dai, A template-free solvent-mediated synthesis of high surface area boron nitride nanosheets for aerobic oxidative desulfurization, Chem. Commun. 52 (2016) 144–147, https://doi.org/10.1039/c5cc07830j.

[40] A. Rajendran, H.X. Fan, J. Feng, W.Y. Li, Desulfurization on boron nitride and boron nitride-based materials, Chem. Asian J. 15 (2020) 2038–2059, https://doi.org/10.1002/asia.202000479.

[41] W. Lei, V.N. Mochalin, D. Liu, S. Qin, Y. Gogotsi, Y. Chen, Boron nitride colloidal solutions, ultralight aerogels and freestanding membranes through one-step exfoliation and functionalization, Nat. Commun. 6 (2015) 8849, https://doi.org/10.1038/ncomms9849.

[42] P. Wu, S. Yang, W. Zhu, H. Li, Y. Chao, H. Zhu, H. Li, S. Dai, Tailoring N-terminated defective edges of porous boron nitride for enhanced aerobic catalysis, Small 13 (2017) 201701857, https://doi.org/10.1002/smll.201701857.

[43] J. Xiong, W. Zhu, H. Li, L. Yang, Y. Chao, P. Wu, S. Xun, W. Jiang, M. Zhang, H. Li, Carbon-doped porous boron nitride: metal-free adsorbents for sulfur removal from fuels, J. Mater. Chem. A 3 (2015) 12738–12747, https://doi.org/10.1039/c5ta01346a.

[44] R. Han, J. Diao, S. Kumar, A. Lyalin, T. Taketsugu, G. Casillas, C. Richardson, F. Liu, C.W. Yoon, H. Liu, X. Sun, Z. Huang, Boron nitride for enhanced oxidative dehydrogenation of ethylbenzene, J. Energy Chem. 57 (2021) 477–484, https://doi.org/10.1016/j.jechem.2020.03.027.

[45] Q. Li, X. Wang, Z. Xie, X. Peng, L. Guo, X. Yu, X. Yang, Z. Lu, X. Zhang, L. Li, Polar bonds induced strong Pd-support electronic interaction drives remarkably enhanced oxygen reduction activity and stability, Appl. Catal. B Environ. 305 (2022), https://doi.org/10.1016/j.apcatb.2021.121020.

[46] C. Wu, B. Wang, N. Wu, C. Han, X. Zhang, S. Shen, Q. Tian, C. Qin, P. Li, Y. Wang, Molecular-scale understanding on the structure evolution from melamine diborate supramolecule to boron nitride fibers, Ceram. Int. 46 (2020) 1083–1090, https://doi.org/10.1016/j.ceramint.2019.09.075.

[47] J. Luo, Y. Wei, Y. Chao, C. Wang, H. Li, J. Xiong, M. Hua, H. Li, W. Zhu, Engineering dual oxygen simultaneously modified boron nitride for boosting adsorptive desulfurization of fuel, Engineering 14 (2022) 86–93, https://doi.org/10.1016/j.eng.2020.08.030.

[48] Q. Weng, D.G. Kvashnin, X. Wang, O. Cretu, Y. Yang, M. Zhou, C. Zhang, D.-M. Tang, P.B. Sorokin, Y. Bando, D. Golberg, Tuning of the optical, electronic, and magnetic properties of boron nitride nanosheets with oxygen doping and functionalization, Adv. Mater. 29 (2017) 1700695, https://doi.org/10.1002/adma.201700695.

[49] L. Dai, Y. Wei, X. Xu, P. Wu, M. Zhang, C. Wang, H. Li, Q. Zhang, H. Li, W. Zhu, Boron and nitride dual vacancies on metal-free oxygen doping boron nitride as initiating sites for deep aerobic oxidative desulfurization, ChemCatChem 12 (2020) 1734–1742, https://doi.org/10.1002/cctc.201902088.

[50] C. Cao, J. Yang, S. Yan, W. Bai, Y. Ma, Y. Xue, C. Tang, Photoelectric and magnetic properties of boron nitride nanosheets with turbostratic structure and oxygen doping, 2D Mater. 9 (2021) 015014, https://doi.org/10.1088/2053-1583/ac37a9.

[51] S. Yang, F. Zhang, Y. Shang, L. Luo, Z. Liu, Highly efficient photocatalytic degradation of refractory organic pollutants onto designed boron nitride: Morphology control and oxygen doping, J. Clean. Prod. 429 (2023) 139532, https://doi.org/10.1016/j.jclepro.2023.139532.

[52] J. Xiong, L. Yang, Y. Chao, J. Pang, P. Wu, M. Zhang, W. Zhu, H. Li, A large number of low coordinated atoms in boron nitride for outstanding adsorptive desulfurization performance, Green Chem. 18 (2016) 3040–3047, https://doi.org/10.1039/c5gc02999f.

[53] C. Gautam, A.K. Yadav, A.K. Singh, A review on infrared spectroscopy of borate glasses with effects of different additives, ISRN Ceram. 2012 (2012) 1–17, https://doi.org/10.5402/2012/428497.
[54] T. Song, J. Dong, R. Li, X. Xu, M. Hiroaki, B. Yang, R. Zhang, Y. Bai, H. Xin, L. Lin, R. Mu, Q. Fu, X. Bao, Oxidative strong metal-support interactions between metals and inert boron nitride, J. Phys. Chem. Lett. 12 (2021) 4187–4194, https://doi.org/10.1021/acs.jpclett.1c00934.
[55] J. Zhu, P. Wu, L. Chen, J. He, Y. Wu, C. Wang, Y. Chao, L. Lu, M. He, W. Zhu, H. Li, 3D-printing of integrated spheres as a superior support of phosphotungstic acid for deep oxidative desulfurization of fuel, J. Energy Chem. 45 (2020) 91–97, https://doi.org/10.1016/j.jechem.2019.10.001.
[56] Y. Xue, P. Dai, X. Jiang, X. Wang, C. Zhang, D. Tang, Q. Weng, X. Wang, A. Pakdel, C. Tang, Y. Bando, D. Golberg, Template-free synthesis of boron nitride foam-like porous monoliths and their high-end applications in water purification, J. Mater. Chem. A 4 (2016) 1469–1478, https://doi.org/10.1039/c5ta08134c.
[57] J. Luo, J. Xiong, Y. Chao, X. Li, H. Li, J. Pang, F. Zhu, W. Zhu, H. Li, Activated boron nitride ultrathin nanosheets for enhanced adsorption desulfurization performance, J. Taiwan Inst. Chem. Eng. 93 (2018) 245–252, https://doi.org/10.1016/j.jtice.2018.07.021.
[58] Z. Yan, J. Lin, X. Yuan, T. Song, C. Yu, Z. Liu, X. He, J. Liang, C. Tang, Y. Huang, Desulfurization of model oil by selective adsorption over porous boron nitride fibers with tailored microstructures, Sci. Rep. 7 (2017) 3297, https://doi.org/10.1038/s41598-017-03600-4.
[59] J. Wang, B. Yang, X. Peng, Y. Ding, S. Yu, F. Zhang, L. Zhang, H. Wu, J. Guo, Design and preparation of polyoxometalate-based catalyst $[MIMPs]_3PMo_6W_6O_{40}$ and its application in deep oxidative desulfurization with excellent recycle performance and low molar O/S ratio, Chem. Eng. J. 429 (2022) 132446, https://doi.org/10.1016/j.cej.2021.132446.
[60] D. Yue, J. Lei, Z. Lina, G. Zhenran, X. Du, J. Li, Oxidation desulfurization of fuels by using amphiphilic hierarchically meso/macroporous phosphotungstic acid/SiO_2 catalysts, Catal. Lett. 148 (2018) 1100–1109, https://doi.org/10.1007/s10562-018-2317-4.
[61] P. Tan, D.M. Xue, J. Zhu, Y. Jiang, Q.X. He, Z. Hou, X.Q. Liu, L.B. Sun, Hierarchical N-doped carbons from designed N-rich polymer: adsorbents with a record-high capacity for desulfurization, AIChE J. 64 (2018) 3786–3793, https://doi.org/10.1002/aic.16357.
[62] H. Li, W. Zhu, S. Zhu, J. Xia, Y. Chang, W. Jiang, M. Zhang, Y. Zhou, H. Li, The selectivity for sulfur removal from oils: an insight from conceptual density functional theory, AIChE J. 62 (2016) 2087–2100, https://doi.org/10.1002/aic.15161.
[63] A. Nisar, Y. Lu, J. Zhuang, X. Wang, Polyoxometalate nanocone nanoreactors: magnetic manipulation and enhanced catalytic performance, Angew. Chem. Int. Ed. 50 (2011) 3187–3192, https://doi.org/10.1002/anie.201006155.
[64] H. Wang, X. Sun, D. Li, X. Zhang, S. Chen, W. Shao, Y. Tian, Y. Xie, Boosting hot-electron generation: exciton dissociation at the order-disorder interfaces in polymeric photocatalysts, J. Am. Chem. Soc. 139 (2017) 2468–2473, https://doi.org/10.1021/jacs.6b12878.